Journal of Sedimentary Research

PROVENANCE OF CENOZOIC INDUS FAN SEDIMENTS (IODP SITES U1456 AND U1457)

--Manuscript Draft--

Manuscript Number:	2019-195R1
Article Type:	Research Article
Corresponding Author:	Eduardo Garzanti Universita di Milano-Bicocca Milano, ITALY
First Author:	Eduardo Garzanti
Order of Authors:	Eduardo Garzanti
	SERGIO ANDO'
	GIOVANNI VEZZOLI
Abstract:	Provenance analysis of IODP Expedition 355 cores in the Laxmi Basin sheds new light on the erosional evolution of the Himalayan belt and its western syntaxis during the Neogene and on large-scale mass-wasting and magmatic events that affected the western continental margin of India in the mid-Miocene and early Paleocene. In the cored Laxmi Basin succession, heavy minerals are far less affected by selective diagenetic dissolution than in foreland-basin sandstones exposed along the Himalayan front. Occurrence of euhedral aegirine and apatite in lower Paleocene mudrocks can be tied to alkaline volcanism affecting the adjacent western Indian margin during the late stage of Deccan activity. In the mid-Miocene Nataraja Slide (the second-largest mass-transport deposit reported from passive margins worldwide), dominant carbonate detritus and depleted heavy-mineral suites (including apatite, garnet, and locally augite or rare aegirine) reveal gravitational failure and sliding of the entire succession of carbonate and siliciclastic Paleogene to lower Neogene strata originally accumulated offshore of the Saurashtra margin of western India. Contrary to previous inferences, reworking of Indus-derived detritus by the slide was negligible. The overlying upper Miocene/lower Pleistocene turbidite package has the same feldspatho-litho-quartzose to litho-feldspatho-quartzose signature of modern Indus fluvio-deltaic sand, indicating that amphibolite-facies metamorphic rocks have been widely exposed in the Himalaya-Karakorum orogen since at least the mid-Miocene. Pleistocene nannofossil oozes with planktonic foraminifera at the top of the fan contain a very subordinate litho-feldspatho-quartzose terrigenous fraction including augitic clinopyroxene, suggesting mixing of dominant biogenic debris with minor detritus contributed both by the Indus River and by a river draining western peninsular India, possibly the paleo-Narmada or the paleo-Tapti.

PROVENANCE OF CENOZOIC INDUS FAN SEDIMENTS

(IODP SITES U1456 AND U1457)

EDUARDO GARZANTI*, SERGIO ANDO'*, AND GIOVANNI VEZZOLI

Laboratory for Provenance Studies, Department of Earth and Environmental Sciences, University of Milano-Bicocca, Milano 20126, Italy

* Corresponding authors (e-mail: sergio.ando@unimib.it and eduardo.garzanti@unimib.it)

Keywords: Sedimentary petrology; Western Himalayan Syntaxis; Indus Delta and Fan; Hydraulic sorting and diagenesis; Nataraja Slide; Paleocene alkaline volcanism; Cenozoic.

ABSTRACT: Provenance analysis of IODP Expedition 355 cores in the Laxmi Basin sheds new light on the erosional evolution of the Himalayan belt and its western syntaxis during the Neogene and on large-scale mass-wasting and magmatic events that affected the western continental margin of India in the mid-Miocene and early Paleocene. In the cored Laxmi Basin succession, heavy minerals are far less affected by selective diagenetic dissolution than in foreland-basin sandstones exposed along the Himalayan front. Occurrence of euhedral aegirine and apatite in lower Paleocene mudrocks can be tied to alkaline volcanism affecting the adjacent western Indian margin during the late stage of Deccan activity. In the mid-Miocene Nataraja Slide (the second-largest mass-transport deposit reported from passive margins worldwide), dominant carbonate detritus and depleted heavy-mineral suites (including apatite, garnet, and locally augite or rare aegirine) reveal gravitational failure and sliding of the entire succession of carbonate and siliciclastic Paleogene to lower Neogene strata originally accumulated offshore of the Saurashtra margin of western India. Contrary to previous inferences, reworking of Indus-derived detritus by the slide was negligible. The overlying upper Miocene/lower Pleistocene turbidite package has the same feldspatho-litho-quartzose to litho-feldspatho-quartzose signature of modern Indus fluvio-deltaic sand, indicating that amphibolite-facies metamorphic rocks have been widely exposed in the Himalaya-Karakorum orogen since at least the mid-Miocene. Pleistocene nannofossil oozes with planktonic foraminifera at the top of the fan contain a very subordinate litho-feldspatho-quartzose terrigenous fraction including augitic clinopyroxene, suggesting mixing of dominant biogenic debris with minor detritus contributed both by the Indus River and by a river draining western peninsular India, possibly the paleo-Narmada or the paleo-Tapti.

"*We ourselves see in all rivers and oceans. It is the image of the ungraspable phantom of life; and this is the key to it all.*" Herman Melville, Moby-Dick; or, The Whale (ch.1, Loomings)

INTRODUCTION

This provenance study of Cenozoic deep-sea sediments of the Laxmi Basin (Fig. 1; central-eastern Arabian Sea) that were cored during IODP Expedition 355 (Pandey et al. 2016a, 2016b) presents the first detailed petrographic and mineralogical analysis of Indus Fan deposits since pioneering work on samples collected during DSDP Leg 23 and ODP Leg 117 at the southeastern and western edges of the fan (Jipa and Kidd 1974; Mallik 1978; Suczek and Ingersoll 1985; Weedon and McCave 1991). Our main aim is to identify changes in sediment provenance from the Himalayan-Karakorum Range *versus* the western Indian continent and continental margin, as a means to reconstruct the Cenozoic paleotectonic and erosional evolution of the region. A more specific sedimentological goal of this study is to verify whether, to what extent, and by which hydrodynamic factors sand composition is modified in the terminal tract of the Indus sediment-routing system and across the transition from the river delta to the deep-sea fan. The impact of selective post-depositional dissolution of less durable minerals on detrital modes of more deeply buried turbidite layers was also investigated. Such an effect is best isolated and assessed in sedimentary successions deposited at the mouth of a large river system, for which provenance may be assumed as a first approximation to have remained roughly constant through time. Discriminating among specific detrital sources within the Himalayan-Karakorum orogen, instead, is beyond the scope of this article. To tackle this thorny task with new epistemic weapons we need first to carefully assess the variability of detrital modes in diverse parts of the Indus source-to-sink system, including the Thal and Thar deserts of Pakistan (Fig. 2; Liang et al. 2019; Garzanti et al. 2020). A deeper understanding of provenance signals and of the processes controlling their pre-depositional and post-depositional modifications is essential to extrapolate the knowledge acquired on modern sedimentary systems in our attempt to reconstruct paleogeographic and paleogeodynamic scenarios based on the compositional information obtained from ancient sandstone suites.

GEOLOGICAL FRAMEWORK

The Indus River and the western Himalaya

The Indus River (~3000 km long; basin area ~10^6 km^2) flows from Tibet to the Arabian Sea mostly through arid land (Fig. 2), where the bulk of rainfall is brought in by the summer monsoon (Rehman et al. 1997; Clift and Plumb 2008). The huge network of large dams and linked canals built in the last century for agriculture and hydropower to meet the needs of a fast-growing population has drastically decreased water discharge from > 150 to < 45 km^3/a, and sediment fluxes from > $300 \cdot 10^6$ t/a to virtually zero at the delta (Inam et al. 2007).

In southwestern Tibet, the Indus River flows westwards along the suture zone and Transhimalayan forearc basin (Garzanti and Van Haver 1988; Henderson et al. 2010), where its northern tributaries drain the Ladakh batholith and its southern tributaries the metamorphic and sedimentary rocks of the Greater and Tethys Himalaya (Munack et al. 2014). Next, the Indus cuts across the western Himalayan Syntaxis, where it receives large volumes of sediment from the Karakorum Range and Kohistan arc in the north and from the Nanga Parbat massif in the south (Fig. 2). The river turns south across the Potwar Plateau and the Salt Range, and enters the foreland basin, where it is joined from the east by major Himalayan rivers of the Punjab and from the west by minor tributaries draining largely Mesozoic carbonate rocks exposed in the Sulaiman and Kirthar ranges of western Pakistan (Fig. 2). Finally, the river reaches the Arabian Sea, where Indus sediments have been accumulating in a deep-sea fan since the Paleogene (Clift et al. 2001). Because of rapid transport from areas of high relief and negligible chemical weathering in arid climates, detrital signatures of modern sand faithfully reflect the lithology of source terranes (Garzanti et al. 2005).

The Laxmi Basin succession

Between the latest Cretaceous and the early Paleocene, central western India was covered by the Deccan Traps basaltic flows, extending seaward to the Laxmi Basin (Todal and Edholm 1988; Krishna et al. 2006; Calvès et al. 2011). The base of the sedimentary succession cored at Site U1457 during IODP Expedition 355 is represented by low-Ti subalkalic tholeiitic basalts (Pandey et al. 2016b, 2019). The overlying 30 m-thick interval of brown and dark gray claystone (Unit V in Fig. 3) contains smectite and traces of volcanic glass (Pandey et al. 2016b p.14/49). Nannofossil assemblages, moderately preserved in the upper part (1062.2–1092.3 m below sea floor, abbreviated as *bsf* throughout the article), include abundant *Coccolithus pelagicus,* common *Cruciplacolithus primus* and *C. tenuis,* together with rare *Prinsius* spp. The presence of *Ellipsolithus macellus* and absence of *Fasciculithus* spp. indicates Zone NP4 and an early Paleocene (Danian) age (63.3-62.1 Ma; Pandey et al. 2016b p.20-21/49).

A major hiatus spanning as much as ~50 million years separates these sediments from the overlying mass-transport deposit (Nataraja Slide), which consists of calcarenite breccias with siliciclastic intercalations and exceeds in volume all but one gravity-flow deposits reported from passive margins worldwide (Calvès et al. 2015; Dailey et al. 2020). Dark-gray sandstone and silty sandstone interbedded with silty shale and lying just below a thin layer of carbonate breccia at the base of Hole U1456E (1101.7-1104.5 m *bsf*) may represent the last *in situ* sediment below the mass-transport deposit. Ranging in thickness between ~227 m (Site U1457) and >350 m (Site U1456), the Nataraja Slide is dated biostratigraphically as just older than 10.8 Ma (i.e., earliest Tortonian; Unit IV in Fig. 3).

The Nataraja Slide is overlain by the 610-760 m-thick main body of Indus Fan turbidites, made of centimetric to plurimetric sand intervals with intercalated mud and ranging in age from late Miocene to early Pleistocene (Units III and II in Fig. 3). An unconformity spanning ~2.0 million years and including the whole of the early Pliocene was identified at ~470 m *bsf* in the upper part of lithologic Unit III (Pandey et al. 2016a p.25/61). The fan is capped by 72-121 m of light-brown to greenish nannofossil ooze dated as late early Pleistocene to Holocene, interbedded with clay and graded layers of silt and sand with sharp basal contact (Unit I; Fig. 3).

METHODS

Sample set

To reconstruct the sedimentary evolution of the Laxmi Basin, we carried out high-resolution petrographic and heavy-mineral analyses on sediment samples collected during IODP Expedition 355 to the Arabian Sea and on modern sand carried by the Tapti River across western India (Fig. 1). New data on 17 samples of turbidite sand ranging in age from mid-Miocene to lower Pleistocene supplemented by heavy-mineral analyses of three samples of Pleistocene ooze, five samples of the middle/late Miocene Nataraja Slide, and four samples of lower Paleocene strata (three claystones and one hyaloclastite) are presented here and integrated with heavy-mineral data on another 22 turbidite samples illustrated and discussed in Andò et al. (2019). The comparison of this dataset with results previously obtained by the same operators and with the same techniques on ten modern samples in the last 750 km of the Indus River course downstream of the Punjab plain (Garzanti et al. 2005), and on nine sediment samples in the Keti Bandar and Thatta boreholes cored in the Indus Delta and covering the last 20 ka (Clift et al. 2010), allowed us to assess the modification of compositional signatures during long-distance fluvio-deltaic to turbiditic transport in the huge Indus sedimentary system. Mineralogical changes caused by burial diagenesis were also investigated. Full information on the considered sample set is provided in Appendix Table A1.

Framework petrography and grain size

A quartered fraction of each sample was impregnated with Araldite, cut into a standard thin section stained with alizarine red to distinguish dolomite and calcite, and analysed by counting 450 points under the petrographic microscope (Gazzi-Dickinson method; Ingersoll et al. 1984). Sands and sandstones are classified by their framework composition according to the relative abundance of the three main groups of components (Q = quartz; F = feldspars; L = lithic fragments), considered where exceeding 10%QFL. According to standard use, the less abundant component goes first, the more abundant last (e.g., in a litho-feldspatho-quartzose sand Q > F > L > 10%QFL; Garzanti 2019a). Very low-rank to low-rank metamorphic lithics are subdivided into metasedimentary and metavolcanic categories, and medium-rank to high-rank metamorphic lithics into felsic (metapelite, metapsammite, metafelsite) and mafic (metabasite) categories (Garzanti and Vezzoli 2003). Median grain size was determined in thin section by ranking the samples from coarsest to finest, followed by visual comparison with in-house standards sieved at 0.25 ϕ sieve interval. The complete petrographic dataset is provided in Appendix Table A2.

Heavy minerals

A quartered aliquot of each bulk-sediment sample was wet sieved with a hand-made 15 μm nylon sieve and a standard 500 μm sieve in steel. Heavy minerals were separated from the 15-500 μm class thus obtained by centrifuging in sodium polytungstate (density 2.90 g/cm^3) and recovered after partial freezing of the test tube with liquid nitrogen. To obtain real volume percentages, $\geq$ 200 transparent heavy minerals were point-counted under a polarizing microscope following a grid of equally spaced points along equally spaced linear traverses (Galehouse 1971; see figure 4 in Garzanti and Andò 2019). All uncertainly determined grains were checked with Raman spectroscopy (Andò and Garzanti 2014). For the three lower Paleocene claystones, heavy minerals were recovered from the 5-500 μm fraction and identified by systematic grain-by-grain coupling of Raman spectroscopy and observations under the polarizing microscope. In order to recover a clean 5-500 μm fraction from these claystones, we first separated the >5 μm fraction from the <5 μm fraction with the pipette method and next sieved the >5 μm fraction thus obtained with a hand-made nylon sieve with 5 μm mesh (Andò 2020).

Transparent heavy-mineral assemblages, called for brevity “tHM suites” throughout the text, are defined as the spectrum of terrigenous extrabasinal minerals with density > 2.90 g/cm^3 identifiable under a transmitted-light microscope. According to the percentage of transparent heavy minerals in the sample (tHMC = transparent heavy mineral concentration; Garzanti and Andò 2007), tHM suites are defined as extremely poor (tHMC < 0.1), very poor (0.5 ≤ tHMC < 1), poor (0.5 ≤ tHMC <1), moderately poor (1 ≤ tHMC <2), moderately rich (2 ≤ tHMC <5), rich (5 ≤ tHMC < 10), or very rich (10 ≤ tHMC < 20). The ZTR index, expressing the chemical durability of the tHM suite (Garzanti 2017), is the sum of zircon, tourmaline and rutile over total transparent heavy minerals (Hubert 1962). Significant minerals are listed in order of abundance (high to low) throughout this article. The complete heavy-mineral dataset is provided in Appendix Table A3.

“True” vs. “false” heavy minerals and the problem of contamination

In sediments, the “heavy fraction” represented by grains denser than 2.90 g/cm^3 contains particles of diverse origin, and it is hard to find a useful objective criterion to precisely discriminate between what should and what should not be included in the heavy-mineral string. Rock fragments and phyllosilicate flakes (chlorite, biotite), although of terrigenous extrabasinal origin and very commonly found in the heavy fraction, are not considered as heavy minerals proper because of their relatively low density and/or platy shape and consequently low settling velocity (Garzanti et al. 2008). Also excluded are grains of presumed or possible intrabasinal origin (e.g., bioclasts, glaucony, biogenic phosphates, vegetal debris, soil particles, Fe-oxide aggregates), diagenetic origin in ancient sandstones (e.g., Ti-oxide aggregates, ferriferous carbonates), or anthropogenic origin in modern sediments (e.g., barite, moissanite) (Garzanti and Andò 2019). The problem is particularly thorny for core samples and cuttings recovered during drilling of ancient strata, which may be contaminated either by caving of lithologies from higher in the well bore or by minerals inherently present in the drilling mud system (Morton and McGill 2018 p.6/29).

In this study, the issue is most relevant for samples cored from the Nataraja Slide and from the lower Paleocene interval at the base of the sedimentary succession, where heavy minerals are invariably very rare. In particular, the sporadic presence of locally common barite or moissanite grains in the fraction denser than 2.90 g/cm^3 suggests that the possibility of contamination needs to be carefully considered in the interpretation of tHM suites contained in these stratigraphic intervals.

PETROGRAPHY AND HEAVY MINERALS

Here we illustrate original petrographic and heavy-mineral data on sediments cored during IODP Expedition 355 at Sites U1456 and U1457 (Fig. 3) and summarize previously published data from the lower course of the Indus River and its delta. Original data on modern Tapti River sand are also presented.

Indus Fan top (Pleistocene)

The topmost part of the Laxmi Basin succession (2.8 m, 20 m, and 75 m *bsf* in Hole U1456A) includes bioclastic oozes with planktonic foraminifera, phosphatic peloids, subordinate benthic foraminifera, sporadic bryozoans, superficial ooids, and glaucony (Fig. 4A). The very fine sand fraction, representing 10-20% of framework grains, is litho-feldspatho-quartzose. The moderately poor tHM suite includes green and subordinately brown augitic clinopyroxene associated with mostly blue-green amphibole, epidote, minor titanite, apatite, garnet, and rare rutile, tourmaline, Cr-spinel and hypersthene (Fig. 5A).

Indus Fan main turbidite body (upper Miocene-lower Pleistocene)

Mostly fine-grained sandy turbidites sampled between 140 and 776 m *bsf* in Holes U1456 A, C, and D are feldspatho-litho-quartzose or litho-feldspatho-quartzose, with plagioclase > K-feldspar (Fig. 6A). Lithic fragments are mainly carbonate (limestone > dolostone), shale/siltstone, and low-rank to high-rank metapelite/metapsammite (Fig. 6B). Granitoid, low-rank metavolcanic, high-rank metabasite, and mainly felsitic volcanic rock fragments occur, together with rare serpentinite grains. Mica (dominantly biotite) represents 26-29% of framework grains in very fine sand (Fig. 4B) and 4-12% in fine sand (Fig. 4C). Mostly rich tHM-suites consist on average of ~51% (43-59%) mostly blue-green amphibole, ~27% (21-35%) epidote-group minerals, and ~6% (1-11%) garnet, with minor diopsidic clinopyroxene, titanite, apatite, and very minor tourmaline, chloritoid, mainly fibrolitic sillimanite, hypersthene, kyanite, zircon, rutile and staurolite (Fig. 5B). Heavy-mineral concentration tends to increase in coarser samples, where high-density garnet tends to increase and lower-density amphibole to decrease.

Nataraja Slide (lowermost Tortonian?)

The Nataraja submarine slide consists of matrix-supported carbonate breccia including blocks of shallow-water limestone slumped from the outer continental shelf of western India, alternating with calcarenite or hemipelagic mudstone and capped by siliciclastic silt turbidites. The studied samples, which are mainly packstones or wackestones with planktonic foraminfera and calcareous algae (Fig. 4D), contain limestone clasts with benthic foraminifera (miliolids, large rotaliids), echinoderms, red algae, locally common radiolaria, rare bivalves, hermatypic corals, bryozoans, mudclasts, glaucony, dolomite rhombs, and phosphate particles (most of them fish teeth; Fig. 5C). The occurrence of the large benthic foraminifer *Lockhartia* and peyssoneliacean red-alga *Polystrata alba* indicates that the eroded limestones were largely of Paleogene age (Dailey et al. 2020). These samples contain 1-5% siliciclastic fraction, with extremely poor tHM-suites including garnet, apatite, epidote, titanite, tourmaline, chloritoid, amphibole, augitic clinopyroxene, barite, Cr-spinel, zircon, rutile, kyanite, staurolite, anatase, and andalusite (ZTR 10-20; Fig. 6C).

Basal turbidite (mid-Miocene)

The 2 m-thick turbiditic interval underlying the Nataraja Slide and retrieved from the bottom of Hole 1456E (sample 56E19, 1102 m *bsf*) is a fine feldspatho-quartzose sand (Fig. 4E), similar to turbidites overlying the Nataraja Slide but somewhat richer in lithic fragments and characterized by a moderately rich tHM suite with a notably higher epidote/amphibole ratio than in the main turbidite body (1.5 *vs.* 0.4-0.7; Fig. 6D). A single specimen of *Sphenolithus heteromorphus* identified in Hole

1456E at 1103.7 m *bsf* constrains the age between 17.7 (late Burdigalian) and 13.5 Ma (early Serravallian), or younger if the specimen is reworked (Pandey et al. 2016a p.28/61).

Volcaniclastic mudrocks (lower Paleocene)

The dense fraction of the four studied samples collected in the 30 m-thick mudrock interval overlying the basaltic basement of the Laxmi Basin, which also includes a hyaloclastite layer (Fig. 4F), mostly consists of carbonate grains, phospate particles (most of them fish teeth), framboidal pyrite, sphalerite, and locally common barite or sparse moissanite of presumed anthropogenic origin (Fig. 5E). The recovered tHM suites are extremely depleted (tHMC mostly ≤ 0.05) but varied. The tHM signature of samples 57C95a (hyaloclastite) and 57C95b closely resembles that of the overlying Neogene turbidites, with a little more zircon, tourmaline, and rutile (ZTR 11-17 *vs.* mostly ≤ 3) (Fig. 6C, 6D). A similar suite characterizes sample 57C93, which however includes several euhedral aegirine grains and rare glaucophane. Euhedral apatite crystals of probable volcanic origin dominate the tHM suite of sample 57C94 and volcanic glass occurs in sample 57C95b. Sample 57C95a contains grains of metamictic zircon, Fe-glaucophane, and Mg-rich or Cr-rich garnet (Fig. 5E).

Indus River and Delta (Holocene)

Modern sand carried by the Indus River in the lower 750 km downstream of the confluence with the Himalayan-derived Punjab rivers ranges in composition from litho-feldspatho-quartzose to feldspatho-quartzo-lithic with plagioclase ≥ K-feldspar and mainly carbonate (limestone > dolostone) and low-rank to high-rank metasedimentary rock fragments (Fig. 6A, 6B). Granitoid, metavolcanic, and metabasite rock fragments are subordinate, volcanic rock fragments and chert minor, and serpentinite grains rare. Mica represents ~3% (2-5%) of framework grains. Mostly rich tHM-suites consist on average of ~50% (41-61%) mostly blue-green amphibole, ~25% (17-35%) epidote-group minerals, and ~12% (6-17%) garnet, with minor diopsidic clinopyroxene, titanite, and tourmaline (Fig. 6C, 6D).

In the Indus delta, uppermost Pleistocene to Holocene sand from the Keti Bandar and Thatta boreholes (Fig. 2; Clift et al. 2010) ranges in composition from litho-feldspatho-quartzose to feldspatho-litho-quartzose with similar plagioclase/K-feldspar ratio and spectrum of lithic fragments as Indus River sand (Fig. 6A, 6B). Mica is, however, notably more common, representing on average ~16% (7-32%) of framework grains (Fig. 3). Mostly moderately rich tHM-suites consist on average of ~52% (45-62%) mostly blue-green amphibole, ~27% (21-35%) epidote-group minerals, and ~6% (2-13%) garnet, with minor diopsidic clinopyroxene, tourmaline, and titanite.

Tapti River (modern sand)

Sand carried by the Tapti River is feldspatho-lithic volcaniclastic, dominated by lathwork grains and plagioclase derived from Deccan Trap basalts, with only a few quartz grains and carbonate rock fragments supplied from sedimentary strata (Fig. 3). The extremely rich tHM suite is dominated by green and subordinately brown augitic clinopyroxene, with minor zircon, very minor blue-green amphibole and epidote, and rare titanite, sillimanite and rutile (ZTR 9; Fig. 6C, 6D).

PROVENANCE

The dataset presented in this study, integrated with previously obtained heavy-mineral data from IODP Sites U1456 and U1457 (Bratenkov et al. 2016; Andò et al. 2019), allows us to accurately reconstruct the Cenozoic erosional evolution of source areas. Although the composition of the main turbidite body is largely monotonous and barely distinguishable from fluvio-deltaic Indus sediments, documenting a clear Himalayan origin (Fig. 3), siliciclastic detritus has distinct mineralogical signatures in the Quaternary fan top, mid-Miocene Nataraja Slide, and lower Paleocene mudrocks, revealing prominent changes in sediment provenance (Fig. 6).

Fan-top oozes

The very subordinate terrigenous fraction of Pleistocene oozes mantling the top of the Indus Fan has litho-feldspatho-quartzose composition comparable to Indus River sand and Indus Fan turbidites, pointing to Himalayan provenance (Fig. 6A, 6B). The tHM suite, however, is sharply distinct and characterized by abundant augitic clinopyroxene (Fig. 6C). A simple forward-mixing calculation (Garzanti et al. 2012) indicates that not more than half of the tHM suite was Indus-derived, whereas the other half was supplied from peninsular India including Deccan volcanic rocks. Reworking of very-fine-grained and mostly bioclastic sediments by bottom currents in the deep sea, and mixing with a terrigenous fraction ultimately derived largely from the Indus mouth but subordinately also supplied by a paleo-Tapti or paleo-Narmada river draining peninsular India, is thus suggested.

Main turbidite body

The upper Miocene to lower Pleistocene Indus Fan turbidites have virtually identical mineralogy as sand delivered today by the Indus fluvio-deltaic system (Fig. 3). Although this observation may not come as a surprise, it has notable implications for our understanding of the Neogene evolution of the Himalayan-Karakorum orogen. Remarkably constant signatures of detritus supplied by the Indus River from the late Miocene to the Pleistocene indicate that the main structural features of the Himalayan range and its western syntaxis were already formed and largely exhumed by Tortonian times, and that the Indus River system has not undergone major drainage reorganizations since then. This is consistent with the petrographic signatures of Miocene foreland-basin strata of northern Pakistan, including abundant feldspars and volcanic lithics, followed by abundant blue-green hornblende, which led to the inference that growth and incipient exhumation of the western Himalayan syntaxis and final development of the Indus drainage took place between the Burdigalian (18-14 Ma; Najman et al. 2003) and the earliest Tortonian (~11 Ma; Cerveny et al. 1989).

Nataraja Slide

The Nataraja Slide documents multiple episodes of catastrophic failure of the western Indian margin during the mid-Miocene. The origin of the gigantic submarine mass transport is traced to a slump scar located ~500 km to the north of Site U1456, between the Saurashtra margin and the Saurashtra high (Fig. 1; Calvès et al. 2015; Nair and Pandey 2018; Dailey et al. 2020). Sediment composition, markedly distinct from the underlying and overlying siliciclastic turbidites, is characterized by dominant carbonate debris including abundant reworked bioclasts of mixed Paleogene to early–middle Miocene age (Pandey et al. 2016a p.26-28/61; 2016b p.20/49). The garnet-apatite-epidote tHM suite, very poor even if referred to the minor siliciclastic fraction only, is also markedly distinct from all older and younger strata. This tHM suite is similar, instead, to the tHM suite of lower Paleocene sandstones of the Tethys Himalaya zone, which were derived from peninsular India and deposited along the northern edge of the Indian passive continental margin (Table 1). The major differences are the higher ZTR index and complete lack of ferromagnesian minerals in the latter, which can be largely explained by the more extensive diagenetic dissolution and anchimetamorphism of Tethys Himalayan strata (Garzanti and Brignoli 1989; Garzanti and Hu 2015). The siliciclastic fraction in the Nataraja Slide was, thus, most likely derived originally from the Indian subcontinent, with contribution from the Deccan Traps indicated by locally common clinopyroxene (Fig. 5C), apatite, and minor Cr-spinel. Based on integrated bulk-sediment geochemistry, heavy-mineral, clay-mineralogy, Nd and Sr isotope-geochemistry data, and 51 detrital zircon U-Pb ages, Dailey et al. (2020 p.100) concluded that "*much of this material may be reworked Indus-derived sediment, with input from western Indian rivers (e.g., Narmada and Tapti Rivers), and some material from the Deccan Traps*". Although the giant mass transport may well be conceived to have induced resuspension, reworking, and mechanical mixing with Indus-derived turbidites, petrographic and heavy-mineral signatures do not show evidence of such a process, and Himalayan-derived detritus within the slide is negligible, if any. The overwhelming abundance of carbonate material, including Paleogene faunas (Fig. 4D), indicates that the gravitational failure affected the western Indian shelf-edge and slope, where siliciclastic sediment delivery at that time was minor. This is independently suggested by the relative abundance of fish teeth and other biogenic phosphates (Fig. 5C), which account for more than half of the very poor dense detrital fraction, indicating that the slide involved offshore sediments accumulating very slowly on the distal shelf and slope. Mineralogical evidence thus suggests that the very sparse siliciclastic detritus involved in the Nataraja Slide originated from reworking of largely lower Paleocene semiconsolidated sandstones lying at the base of the Paleogene carbonate succession of the western Indian continental margin rather than from Indus-derived turbidites.

Heavy minerals in the Nataraja Slide are commonly superficially corroded (e.g., orange-peel garnet in Fig. 5C), indicating a strong diagenetic overprint, and the tHM suite is invariably much poorer in amphibole (< 10%tHM) than in the overlying (43-59%tHM) and even underlying (33%tHM) Indus Fan turbidites. Diagenetic dissolution leading to selective chemical breakdown of amphibole, therefore, did not occur in the Laxmi Basin after deposition, but during burial underneath the stratigraphically overlying succession of the western Indian margin before mid-Miocene gravitational collapse.

We conclude that the Nataraja Slide involved the entire lower Paleocene to lower-middle Miocene sedimentary succession of the western Indian continental margin, which was not markedly dissimilar from that presently exposed in the Tethys Himalaya far to the north (Li et al. 2015, 2017, 2020). Evidence for reworking of Himalayan-derived sediments conveyed via the Indus fluvio-deltaic system is lacking.

Basal turbidite

The 2 m-thick turbidite interval underlying the Nataraja Slide has feldspatho-litho-quartzose detrital mode indistinguishable from upper Miocene-lower Pleistocene turbidites above the Nataraja Slide (Fig. 3). The tHM suite is also comparable, but only moderately rich, and with notably higher epidote/amphibole ratio (Fig. 6D), a difference explained by more extensive selective intrastratal dissolution of amphibole in more deeply buried strata (as discussed below). Common amphibole grains in Miocene strata of the Indus Fan, contrary to foreland-basin successions where ferromagnesian minerals have been systematically leached out in strata as young as the Pleistocene (Garzanti 2019b), proves that amphibolite-facies metamorphic rocks were exposed in the Himalaya-Karakorum orogen at that time (White et al. 2002; Najman et al. 2009).

Volcaniclastic mudrocks

The extremely poor dense fraction recovered from lower Paleocene mudrocks and interlayered hyaloclastite reveals a mixture of particles of different origin (Fig. 5E). All four analysed samples contain amphibole and epidote, and some include garnet, chloritoid or staurolite grains in proportions not dissimilar from that in Neogene Indus Fan turbidites and in the modern Indus River system. Because these layers were deposited a couple of million years before the onset of the India-Asia continental collision (Hu et al. 2015, 2016), a Himalayan provenance is excluded, and the presence of barite and moissanite grains suggests anthropogenic contamination. The possibility of downhole contamination during drilling is supported by forward mixing calculations, which indicate that such an extremely depleted tHM assemblage can be reproduced as a mixture of the tHM suites contained in the main turbidite body and in the Nataraja Slide in proportion 85:15. Inadvertent contamination during sample treatment in our laboratory is unlikely because sieves were made expressly for each new sample and particular care was taken at each step. Moreover, virtually the same tHM suite was obtained from the two samples 57C95a (hyaloclastite; Fig. 4F) and 57C95b, which were prepared and counted in different months (January and October 2019).

If the pseudo-orogenic tHM assemblage mentioned above is considered as spurious and consequently ignored, then the dense fraction in this lower Paleocene interval almost exclusively consists of carbonate and phosphate biogenic debris accumulated at slow rates in offshore marine settings and of authigenic minerals such as framboidal pyrite and possibly barite and sphalerite (e.g., Milliken and Mack 1990), with an extremely poor tHM suite chiefly represented by euhedral crystals of either apatite or clinopyroxene (mostly aegirine; Fig. 5E). These grains are most likely of penecontemporaneous volcanic origin and ejected during the late stages of Deccan volcanism from alkaline centers possibly located along the adjacent western Indian margin ~550 km to the ENE (e,g. Murud area in Fig. 1; Melluso et al. 2002; Dessai and Viegas 2010). The rare grains of pyrope or Cr-rich garnet, Fe-glaucophane, and metamictic zircon might represent xenocrysts ejected during volcanic eruptions (Ohba and Nakagawa 2002).

SUPERPOSED CONTROLS ON COMPOSITIONAL SIGNATURES

Grain-size and hydraulic-sorting

In the main turbidite body of late Miocene to early Pleistocene age (Units III and II), mica increases notably with decreasing grain-size (correlation coefficient -0.82, significance level 0.1%; Fig. 4B vs. 4C), whereas heavy-minerals increase with increasing grain size, higher-density garnet and opaque Fe-Ti-Cr oxides faster than lower-density amphibole. The intersample mineralogical variability is thus largely grain-size dependent.

As noted by Andò et al. (2019), the concentration of heavy minerals in general and particularly of denser garnet and opaque Fe-Ti-Cr oxides is systematically higher in plurimetric sand intervals representing turbiditic channels. Conversely, phyllosilicates are markedly more abundant in centimetric to decimetric silty overbank turbidites. Such partitioning of detrital minerals in different depositional subenvironments chiefly reflects suspension sorting (i.e., sorting by settling velocity during transport; Rouse 1937), with faster-settling denser minerals concentrating towards the base of the turbidity current and slower-settling platy phyllosilicates concentrating in suspension.

Mineralogical changes from the land to the ocean floor

Comparison of detrital modes along the Indus fluvio-deltaic to turbiditic sediment-routing system indicates that, besides the local sedimentary-differentiation effects associated with grain size and hydraulic sorting described above, all compositional fingerprints remain remarkably constant from the river mouth to the deep-sea fan (Fig. 3), as observed also in the Bengal sediment system on the eastern side of peninsular India (Borromeo et al. 2019; Garzanti et al. 2019).

Closer inspection, however, reveals that, grain size being equal, Indus Fan turbiditic sand tends to be poorer in heavy minerals (garnet, and possibly slightly in staurolite and kyanite) than Indus River sand, and richer in phyllosilicates, amphibole, and possibly slightly in epidote and sillimanite (Fig. 3). Differences between Indus Delta and Indus Fan sands are subtler, less evident, and finally blurred for deposits of progressively finer grain size. The tendency to sequester faster-settling denser detrital grains in the fluvio-deltaic system (e.g., garnet) and to concentrate slow-settling minerals offshore (especially phyllosilicates) results from the combination of diverse hydraulic-sorting mechanisms (Komar 2007; Garzanti et al. 2009). Settling equivalence and suspension sorting account for concentration of denser minerals in bedload and, thus, for their preferential deposition in fluvial and turbiditic channels, whereas less dense and platy minerals transported preferentially in suspended load are largely deposited in overbank deposits both on land and in the deep sea. Furthermore, the selective-entrainment process leads to concentration of densest minerals (e.g., garnet, zircon, and magnetite) in placer lags formed in proximal settings, a phenomenon which is particularly manifest in deltaic cusps undergoing accelerated erosion, whereas platy and less dense minerals (e.g., phyllosilicates) are largely winnowed offshore. Therefore, as observed in the Bengal sediment system (Garzanti et al. 2010, 2011, 2019), the same mineralogical differentiation observed vertically at any point within the fluvial channel from bedload to suspended load is reproduced horizontally from coastal to offshore deposits and, finally, from channelized to overbank turbidites in the deep sea, with progressive depletion of dense equant mineral species such as garnet and enrichment in low-density and platy grains such as phyllosilicates.

Diagenetic dissolution

As noted above, detrital modes and tHM suites remain remarkably constant throughout the upper Miocene to lower Pleistocene turbiditic succession cored in the Laxmi Basin (Fig. 3). No mineral abundance correlates significantly with core depth. The abundance of durable zircon does not systematically increase downcore, nor amphibole systematically decreases. The ZTR index remains mostly ≤ 5, as in the modern Indus River and Delta. Transparent-heavy-mineral suites remain mostly moderately rich to rich and pyroxene occurs throughout the interval, although it tends to decrease in abundance with depth in Miocene strata (Fig. 3).

Selective dissolution of a large part of the original unstable ferromagnesian minerals is indicated only for the mid-Miocene turbidite sample 56E19 underlying the Nataraja Slide at 1102 m *bsf*. This sample has a notably poorer, although still moderately rich tHM suite containing common amphibole and a few pyroxene grains, but the epidote/amphibole ratio is notably higher than in turbidites overlying the Nataraja Slide (Fig. 6D).

The few transparent heavy minerals recovered from the lower Paleocene mudrock interval between 1067 and 1085 m *bsf* include aegirine and glaucophane, which confirms that Na-rich ferromagnesian silicates are much more durable than Na-poor varieties during burial diagenesis (Morton and Hallsworth 2007 p.228).

Overall, these observations are similar to observations from other deep-sea sedimentary successions, including those cored in the Bengal and Nicobar Fans, showing that heavy-mineral concentration and the relative proportions among amphibole, epidote, garnet, and ZTR minerals may be maintained in upper Miocene strata buried as much as ~800 m (Morton and Hallsworth 2007; Andò et al. 2012; Garzanti et al. 2018; Pickering et al. 2020). In contrast, Himalayan-derived sedimentary successions exposed along the front of the Himalayan belt are invariably characterized by very poor to moderately poor heavy-mineral suites that may lack amphibole even in strata as young as the Pleistocene (e.g., Szulc et al. 2006). Full provenance information cannot be acquired from these foreland-basin sediments, because they have undergone very extensive chemical breakdown of unstable ferromagnesian minerals during deeper burial and/or during subsequent deformation and exhumation (Garzanti 2019b). Instead, the much better preserved tHM suites of deep-sea-fan deposits allow us to directly extrapolate the rich information obtained from modern-sand petrology at least back to the late Miocene.

SUMMARY

The Cenozoic succession cored during IODP Expedition 355 to the Laxmi Basin can be subdivided into five stratigraphic intervals overlying the basaltic basement (from top to bottom): 1) 72-121 m-thick Pleistocene fan-top sediments; 2) 610-760 m-thick upper Miocene-lower Pleistocene main body of Indus Fan turbidites; 3) 227-380 m-thick Nataraja Slide of probably earliest Tortonian age; 4) 2 m-thick mid-Miocene turbidite underlying the slide; and, 5) 30 m-thick lower Paleocene volcaniclastic mudrocks. Throughout the succession, the original mineralogical assemblages have been far less decimated by diagenetic dissolution than clastic units of the Himalayan foreland basin and, thus, reflect much more faithfully the Neogene erosional evolution of the Himalaya-Karakorum orogen.

Very fine-grained Quaternary fan-top deposits are nannofossil oozes with planktonic foraminifera. The very subordinate litho-feldspatho-quartzose terrigenous fraction includes augitic clinopyroxene, suggesting reworking by bottom currents and mixing of detritus derived largely from the Indus mouth but partly supplied by a paleoriver draining the Deccan Traps flood basalts in peninsular India.

The feldspatho-litho-quartzose to litho-feldspatho-quartzose composition of upper Miocene to lower Pleistocene Indus Fan turbidites is similar to that of modern sand of the Indus River and Delta. Mineralogical fingerprints have remained remarkably constant both in time and space from the river mouth to the deep-sea fan. However, as also observed in the Bengal sediment system, faster-settling denser detrital grains (e.g., garnet) tend to be sequestered in the fluvio-deltaic system, whereas slow-settling minerals (especially phyllosilicates) are preferentially winnowed offshore and deposited in the deep sea. Within the fan, heavy minerals (especially garnet and opaque Fe-Ti-Cr oxides) tend to concentrate in coarser channelized turbidites, and mica flakes in finer overbank deposits. The predominance of amphibole among transparent heavy minerals throughout the upper Miocene to lower Pleistocene, both in the Indus and Bengal-Nicobar Fans, contrasts markedly with the much poorer heavy-mineral suites invariably characterizing the coeval sedimentary rocks deposited along the Himalayan foreland basin. This demonstrates conclusively that amphibolite-facies metamorphic rocks of the Himalaya-Karakorum orogen were widely exposed by the middle Miocene at latest, and that heavy-mineral suites of foreland-basin clastic rocks have been drastically depleted in less stable minerals during diagenesis. Sediments cored in the Laxmi Basin indicate that effects of selective diagenetic dissolution comparable to those observed in Plio-Pleistocene foreland-basin sediments are not reached even in the mid-Miocene turbidite underlying the Nataraja Slide, which is characterized by a moderately rich heavy-mineral suite, including common amphibole although less abundant than epidote.

The Nataraja Slide, the second-largest mass-transport deposit reported from passive margins worldwide, documents a multiple gravitational collapse that involved the entire Paleogene sedimentary succession of the western Indian margin, as indicated by dominant carbonate clasts, mixed faunal assemblages of Paleogene to early–middle Miocene age, and a very minor siliciclastic fraction including an extremely poor heavy-mineral suite similar to that characterizing lower Paleocene Tethys Himalayan sandstones derived from peninsular India. Differently from what had been previously inferred, neither evidence of reworking of Indus Fan turbidites nor significant input from western Indian rivers is indicated in the Nataraja Slide. Finally, the occurrence in lower Paleocene mudrocks of euhedral aegirine and apatite, together with volcanic glass and smectite, points to air-borne tephra ejected from alkaline volcanic centres possibly located along the adjacent western Indian margin during the late stages of Deccan magmatism.

ACKOWLEDGMENTS

This research used samples and data obtained from the International Ocean Discovery Program (IODP), and SA warmly thanks Dhananjai K. Pandey, Peter D. Clift, Denise K. Kulhanek, S.Aharonovic, and all research scientists on board the Joides Resolution for the fruitful and joyful time spent together during IODP Expedition 355. Samples of lower Paleocene mudrocks and of modern Tapti River sands were kindly provided by Denise K. Kulhanek, and by Santanu Banerjee and Xiumian Hu. Funding was supplied by projects MIUR-PRIN 2015EC9PJ5 (The subduction and exhumation of the continental lithosphere: their effects on the structure and evolution of the orogens) and MIUR – Dipartimenti di Eccellenza 2018–2022, Department of Earth and Environmental Sciences, University of Milano-Bicocca. The manuscript benefited from very careful and constructive advice generously provided by Peter Clift and Raymond Ingersoll.

SUPPLEMENTARY MATERIAL

Supplementary data associated with this article, to be found in the online version at http://dx.doi.___________, include information on sampling sites (Table A1) and the complete bulk-petrography (Table A2), and heavy-mineral datasets (Table A3).

FIGURE CAPTIONS

Figure 1. Indus Fan. Shown are locations of IODP Expedition 355 Sites U1456 and U1457 in Laxmi Basin (Pandey et al. 2016a, 2016b), main fluvial entry points of terrigenous detritus, slump scar and areal extent of Nataraja Slide (NS; light blue shade; Dailey et al. 2020), area covered by Deccan volcanic rocks on land and at sea (light purple shade; Carmichael et al. 2009), and Murud alkaline volcanic center along adjacent Indian coast (Melluso et al. 2002). WHS = western Himalayn syntaxis.

Figure 2. Geology of the Indus catchment (mod. after Garzanti et al. 2005) showing the location of the Thatta (T) and Keti Bandar (K) boreholes in the Indus Delta (Clift et al. 2010).

Figure 3. Stratigraphy of IODP Sites U1456 and U1457, with petrographic and heavy-mineral data. Q = quartz; KF = feldspar; P = plagioclase; L = lithic fragments (Lvm = volcanic and low-rank metavolcanic; Lch = carbonate and chert; Lsm = other sedimentary and low-rank metasedimentary; Lmf = high-rank metapelite and metafelsite; Lbu = high-rank metabasite and ultramafic). HM = heavy minerals. ZTR = zircon + tourmaline + rutile; Ap = apatite; Ttn = titanite; Ep = epidote; Grt = garnet; CSKA = chloritoid + staurolite + andalusite + kyanite + sillimanite; Amp = amphibole; Px = pyroxene; &tHM = other transparent heavy minerals.

Figure 4. Petrography of Indus Fan succession in Laxmi basin. **A**: Fan top (56A4, 20 m *bsf*). Main turbidite body (**B**: 56A25, 179 m *bsf*; **C**: 56A57, 326 m *bsf*). **D**) Nataraja Slide (56E15, 1073 m *bsf*). **E**) Turbidite bed at base of Nataraja Slide (56E19, 1102 m *bsf*). **F**) 10 cm-thick hyaloclastite intercalated in lower Paleocene mudrocks (57C95, 1083 m *bsf*). A, B, C, and E with crossed polarizers. Blue bar for scale 100 μm.

Figure 5. Transparent heavy minerals and intrabasinal, authigenic or possibly anthropogenic grains denser than 2.90 g/cm^3 characterizing five stratigraphic intervals identified in Laxmi Basin succession. **A)** Clinopyroxene plausibly derived from Deccan Traps, associated with hypersthene plausibly derived from Kohistan arc and with intrabasinal bioclasts and pellets (56A4, 20 m *bsf*). **B**)

Himalayan-derived heavy minerals including unstable ferromagnesian species corroded to various degrees. **C)** Etched clinopyroxene plausibly derived originally from Deccan Traps, relatively fresh apatite, and garnet showing corroded orange-peel surface associated with glaucony grains and fish teeth indicating slow accumulation rate (56E4, 978 m *bsf*; 56E7, 1000 m *bsf*). **D)** Strongly etched amphibole coexists with corroded epidote, euhedral titanite and fresh Cr-spinel, reflecting different durabilities of detrital minerals to diagenetic dissolution (56E19, 1102 m *bsf*). **E)** Euhedral aegirine (57C93), needle-like apatite (57C94), and glass fragments (57C95b) indicate ejection from alkaline eruptive centres during late stages of Deccan volcanism. Mg-rich and Cr-rich garnets (57C95b) may represent xenocrysts incorporated into volcanic ejecta. Abundance of fish teeth (57C93) indicates slow accumulation rate. Barite (57C95a) may suggest contamination by drilling muds.

Figure 6. Compositional signatures. **A**) Framework petrography (Q = quartz; F = feldspar; L = lithic fragments). **B**) Lithic fragments (Lm = metamorphic; Lv = volcanic; Ls = sedimentary). **C**) Heavy minerals (Amp = amphibole; Ep = epidote; Px = pyroxene; Sp = Cr-spinel; &tHM = garnet and other transparent heavy minerals). **D**) Main heavy minerals in orogenic sediments (Grt = garnet). Detrital modes for modern Tapti River sand indicated in red in ***A*** and ***B***. Data for Indus fluvial and deltaic sands after Garzanti et al. (2005) and Clift et al. (2010).

Table 1. Key petrographic and heavy-mineral parameters. N° = number of samples; Q = quartz; KF = K-feldspar; P = plagioclase; L = lithic grains (Lv = volcanic; Lc = carbonate; &Lsm = other sedimentary and low-rank metasedimentary; Lmf = high-rank metamoprphic: Lbu = metabasite and ultramafic). HM = heavy-minerals; tHMC = transparent heavy-mineral concentration; ZTR = zircon + tourmaline + rutile; Ap = apatite; Ttn = titanite; Ep = epidote-group; Grt = garnet; CSKA = chloritoid + staurolite + andalusite + kyanite + sillimanite; Amp = amphibole; Px = pyroxene; &tHM = other transparent heavy minerals (Cr-spinel, anatase, brookite, monazite, vesuvianite, pumpellyite, prehnite, olivine, diaspore). Data sources: 1 = this study; 2 = Garzanti et al. (2005); 3 = Clift et al. (2010); 4 = Andò et al. (2019); 5 = Bratenkov et al. (2016); 6 = Indian-derived Paleocene sandstones

from the Sangdanlin and Mubala sections of the Tethys Himalayan zone of southern Tibet (Wang et al. 2011; An et al. 2017).

REFERENCES

AN, W., WANG, J.G., GARZANTI, E., AND HU, X.M., 2017, Dating of the India–Asia collision at 61 Ma from the Mubala section in Tibetan Himalaya: 6th Chinese Sedimentological Congress Abstract, Nanjing, 27–30 October 2017.

ANDÒ, S., 2020. Gravimetric separation of heavy-minerals in sediments. Minerals, 10 (3), 273; doi:10.3390/min10030273.

ANDÒ, S., AND GARZANTI, E., 2014, Raman spectroscopy in heavy-mineral studies, *in* Scott, R.A., Smyth. H.R., Morton, A.C., and Richardson, N., eds., Sediment provenance studies in hydrocarbon exploration and production: Geological Society London, Special Publication 386, p. 395-412.

ANDÒ, S., GARZANTI, E., PADOAN, M., AND LIMONTA, M., 2012, Corrosion of heavy minerals during weathering and diagenesis: a catalog for optical analysis: Sedimentary Geology, v. 280, p. 165-178.

ANDÒ, S., AHARONOVICH, S., HAHN, A., GEORGE, S.C., CLIFT, P.D., AND GARZANTI, E., 2019, Integrating heavy-mineral, geochemical, and biomarker analyses of Plio-Pleistocene sandy and silty turbidites: a novel approach for provenance studies (Indus Fan, IODP Expedition 355): Geological Magazine, p. 1-10, doi: 10.1017/S0016756819000773.

BORROMEO, L., ANDÒ, S., FRANCE-LANORD, C., COLETTI, G., HAHN, A., AND GARZANTI, E., 2019, Provenance of Bengal Shelf Sediments: 1. Mineralogy and Geochemistry of Silt: Minerals, v. 9 (10), 640, doi:10.3390/min9100640.

BRATENKOV, S., AND THE EXPEDITION 355 SCIENTISTS, 2016. Multi-proxy geochemical analyses of Indus Submarine Fan sediments sampled by IODP Expedition 355: Implications for sediment provenance and palaeoclimate reconstructions: EGU General Assembly, Geophysical Research Abstracts, v. 18, EGU2016-3735-1, 2016.

CALVÈS, G., SCHWAB, A.M., HUUSE, M., CLIFT, P.D., GAINA, C., JOLLEY, D., TABREZ, A.R., AND INAM, A., 2011, Seismic volcanostratigraphy of the western Indian rifted margin: The pre- Deccan igneous province: Journal of Geophysical Research Solid Earth, v. 116, B01101, doi:10.1029/2010JB000862.

CALVÈS, G., HUUSE, M., CLIFT, P.D., AND BRUSSET, S., 2015, Giant fossil mass wasting off the coast of West India: The Nataraja submarine slide: Earth and Planetary Science Letters, v. 432, p. 265–272.

CARMICHAEL, S.M., AKHTER, S., BENNETT, J.K., FATIMI, M.A., HOSEIN, K., JONES, R.W., LONGACRE, M.B., OSBORNE, M.J., AND TOZER, R.S.J., 2009, Geology and hydrocarbon potential of the offshore Indus Basin, Pakistan: Petroleum Geoscience, v. 15, p. 107–116.

CERVENY, P.F., JOHNSON, N.M., TAHIRKHELI, R.A.K., AND BONIS, N.R., 1989, Tectonic and geomorphic implications of Siwalik group heavy minerals, Potwar plateau, Pakistan, *in* Malinconico, L.L., and Lillie, R.J., eds., Tectonics of the Western Himalayas: Geological Society of America, Special Paper 232, p. 129-136

CLIFT, P.D., AND PLUMB, R.A., 2008, The Asian monsoon: causes, history and effects: Cambridge, Cambridge University Press, v. 288, 270 p.

CLIFT, P.D., SHIMIZU, N., LAYNE, G., BLUSZTAJN, J.S., GAEDICKE, C., SCHLUTER, H.-U., CLARK, M.K., AND AMJAD, S., 2001, Development of the Indus Fan and its significance for the erosional history of the Western Himalaya and Karakoram: Geological Society of America, Bulletin, v. 113, p. 1039-1051.

CLIFT, P.D., GIOSAN, L., CARTER, A., GARZANTI, E., GALY, V., TABREZ, A.R., PRINGLE, M., CAMPBELL, I.H., FRANCE-LANORD, C., BLUSZTAJIN, J., ALLEN, C., ALIZAI, A., LÜCKGE, A., DANISH, M., AND RABBANI M.M., 2010, Monsoon control over erosion patterns in the Western Himalaya: possible feed-backs into the tectonic evolution, *in* Clift, P.D., Tada, R., and Zheng, H., eds., Monsoon evolution and tectonic-climate linkage in Asia: Geological Society, London, Special Publication 342, p. 185-218.

DAILEY, S.K., CLIFT, P.D., KULHANEK, D.K., BLUSZTAJN, J., ROUTLEDGE, C.M., CALVÈS, G., O'SULLIVAN, P., JONELL, T.N., PANDEY, D.K., ANDÒ, S., COLETTI, G., ZHOU, P., LI, Y., NEUBECK, N.E., BENDLE, J.A.P., AHARONOVICH, S., GRIFFITH, E.M., GURUMURTHY, G.P., HAHN, A., IWAI, M., KHIM, B.K., KUMAR, A., KUMAR. A,G., LIDDY, H.M., LU, H., LYLE, M.W., MISHRA, R., RADHAKRISHNA, T., SARASWAT, R., SAXENA, R., SCARDIA, G., SHARMA,G.K., SINGH, A.D., STEINKE, S., SUZUKI, K., TAUXE, L., TIWARI, M., XU, Z., AND YU, Z., 2020, Large-scale mass wasting on the Miocene continental margin of Western India: Geological Society of America Bulletin, v. 132 (1-2), p. 85–112.

DESSAI, A.G., AND VIEGAS, A., 2010, Petrogenesis of alkaline rocks from Murud-Janjira, in the Deccan Traps, western India: Mineralogy and Petrology, v. 98(1-4), p. 297-311.

GALEHOUSE, J.S., 1971, Point counting, *in* Carver, R.E., ed., Procedures in sedimentary petrology: New York, Wiley, p. 385-407.

GARZANTI, E., 2017, The maturity myth in sedimentology and provenance analysis: Journal of Sedimentary Research, v. 87, p. 353-365.

GARZANTI, E., 2019a, Petrographic classification of sand and sandstone: Earth-Science Reviews, v. 192, p. 545-563.

GARZANTI, E., 2019b, The Himalayan foreland basin from collision onset to the present: a sedimentary-petrology perspective, in Treloar, P., and Searle, M.P., eds., Himalayan Tectonics: A Modern Synthesis: Geological Society London, Special Publication 483, p. 65–122, doi: 10.1144/SP483.17.

GARZANTI, E., AND ANDÒ, S., 2007, Heavy-mineral concentration in modern sands: implications for provenance interpretation, in Mange, M.A., and Wright, D.T., eds., Heavy Minerals in Use: Amsterdam, Elsevier, Developments in Sedimentology Series 58, p. 517-545.

GARZANTI, E., AND ANDÒ, S., 2019, Heavy Minerals for Junior Woodchucks: Minerals, v. 9 (3), 148, doi:10.3390/min9030148.

GARZANTI, E., AND BRIGNOLI, G., 1989, Low temperature metamorphism in the Zanskar sedimentary nappes (NW Himalaya, India): Eclogae Geologicae Helvetiae, v. 82, p. 669-684.

GARZANTI, E., AND HU, X., 2015, Latest Cretaceous Himalayan tectonics: Obduction, collison or Deccan-related uplift?: Gondwana Research, v. 28, p. 165-178.

GARZANTI, E., AND VAN HAVER, T., 1988, The Indus clastics: forearc basin sedimentation in the Ladakh Himalaya (India): Sedimentary Geology, v. 59, p. 237-249,

GARZANTI, E., AND VEZZOLI, G., 2003, A classification of metamorphic grains in sands based on their composition and grade: Journal of Sedimentary Research, v. 73, p. 830-837.

GARZANTI, E., VEZZOLI, G., ANDÒ, S., PAPARELLA, P., AND CLIFT, P.D., 2005, Petrology of Indus River sands : a key to interpret erosion history of the Western Himalayan Syntaxis: Earth and Planetary Science Letters, v. 229, p. 287– 302.

GARZANTI, E., ANDÒ, S., AND VEZZOLI G., 2008, Settling equivalence of detrital minerals and grain-size dependence of sediment composition. Earth and Planetary Science Letters, v. 273, p.138-151.

GARZANTI, E., ANDÒ, S., AND VEZZOLI G., 2009, Grain-size dependence of sediment composition and environmental bias in provenance studies: Earth and Planetary Science Letters, v. 277, p. 422-432.

GARZANTI, E., ANDÒ, S., FRANCE-LANORD, C., VEZZOLI, G., AND NAJMAN, Y., 2010, Mineralogical and chemical variability of fluvial sediments. 1. Bedload sand (Ganga-Brahmaputra, Bangladesh): Earth and Planetary Science Letters, v. 299, p. 368-381.

GARZANTI, E., ANDÒ, S., FRANCE-LANORD, C., GALY, V., CENSI, P., AND VIGNOLA, P., 2011, Mineralogical and chemical variability of fluvial sediments. 2. Suspended-load silt (Ganga-Brahmaputra, Bangladesh): Earth and Planetary Science Letters, v. 302, p. 107–120.

GARZANTI, E., RESENTINI, A., VEZZOLI, G., ANDÒ, S., MALUSÀ, M., AND PADOAN, M., 2012, Forward compositional modelling of Alpine orogenic sediments: Sedimentary Geology, v. 280, p. 149–164.

GARZANTI, E., ANDÒ, S., LIMONTA, M., FIELDING, L., AND NAJMAN, Y., 2018, Diagenetic control on mineralogical suites in sand, silt, and mud (Cenozoic Nile Delta): implications for provenance reconstructions: Earth-Science Reviews, v. 185, p. 122-139

GARZANTI, E., ANDÒ, S., FRANCE-LANORD, C., LIMONTA, M., BORROMEO, L., AND VEZZOLI, G., 2019, Provenance of Bengal Shelf Sediments. 2. Petrology of sand: Minerals, v. 9 (10), 642, doi:10.3390/min9100642.

GARZANTI, E., LIANG, W., ANDÒ, S., CLIFT, P.D., RESENTINI, A., VERMEESCH, P., VEZZOLI, G., 2020. Provenance of Thal Desert sand: focused erosion in the western Himalayan syntaxis and foreland-basin deposition driven by latest Quaternary climate change. Earth-Science Reviews, in review.

HENDERSON, A.L., NAJMAN, Y., PARRISH, R., BOUDAGHER-FADEL, M., BARFORD, D., GARZANTI, E., AND ANDÒ, S., 2010, The Geology of the Cenozoic deltasin sedimentary rocks; palaeoenvironmental interpretation of sedimentation from the western Himalaya during the early phases of India-Eurasia collision: Tectonics, v. 29, TC6015, 35 pp., doi:10.1029/2009TC002651.

HU, X., GARZANTI, E., MOORE, T., AND RAFFI, I., 2015, Direct stratigraphic dating of India-Asia collision onset at the Selandian (middle Paleocene, 59±1 Ma): Geology, v. 43, p. 859-862.

HU, X., GARZANTI, E., WANG J-G., HUANG, W., AN, W., AND WEBB, A., 2016, The timing of India-Asia collision onset – facts, theories, controversies: Earth-Science Reviews, v. 160, p. 264-299.

HUBERT, J.F., 1962, A zircon–tourmaline–rutile maturity index and the interdependence of the composition of heavy mineral assemblages with the gross composition and texture of sandstones: Journal of Sedimentary Petrology, v. 32, p. 440–450

INAM, A., CLIFT, P.D., GIOSAN, L., TABREZ, A.R., TAHIR, M., RABBANI, M.M., AND DANISH, M., 2007, The geographic, geological and oceanographic setting of the Indus River, *in* Gupta, A., ed., Large rivers: Geomorphology and Management: Chichester (UK), Wiley, p. 333-345.

INGERSOLL, R.V., BULLARD, T.F., FORD, R.L., GRIMM, J.P., PICKLE, J.D., AND SARES, S.W., 1984, The effect of grain size on detrital modes: A test of the Gazzi-Dickinson point-counting method: Journal of Sedimentary Petrology, v. 54, p. 103–116.

JIPA, D., AND KIDD, R.B., 1974, Sedimentation of coarser grained interbeds in the Arabian Sea and sedimentation processes of the Indus Cone, *in* Whitmarsh, R.B., Weser, O.E., Ross, D.A., et al., eds., Initial Report of the Deep Sea Drilling Project 219-230: Washington, D.C., US Government Printing Office, v. 23, p. 471-495.

KOMAR, P.D., 2007, The entrainment, transport and sorting of heavy minerals by waves and currents, *in* Mange, M.A., and Wright, D.T., eds., Heavy Minerals in Use: Elsevier, Amsterdam, Developments in Sedimentology Series 58, p. 3–48.

KRISHNA, K.S., RAO, D.G., AND SAR, D., 2006, Nature of the crust in the Laxmi Basin (14°-20°N), western continental margin of India: Tectonics, v. 25, TC1006, doi:10.1029/2004TC001747.

LI, J., HU, X., GARZANTI, E., AN, W., AND WANG, J., 2015, Paleogene carbonate microfacies and sandstone provenance (Gamba area, South Tibet): Stratigraphic response to initial India-Asia continental collision: Journal of Asian Earth Sciences, v. 104, p. 39-54.

LI, J., HU, X., GARZANTI, E., AND BOUDAGHER-FADEL, M., 2017, Shallow-water carbonate record of the Paleocene–Eocene thermal maximum and tectonic uplift of the Tethys Himalaya during early India-Asia collision (southern Tibet): Palaeogeography, Palaeoclimatology, Palaeoecology, v. 466, p. 153-165.

LI, J., HU, X.M., GARZANTI, E., BANERJEE, S., AND BOUDAGHER-FADEL, M., 2020, Late Cretaceous topographic doming caused by initial upwelling of Deccan magmas: Stratigraphic and sedimentological evidence: Geological Society of America Bulletin, v. 132(3-4), p. 835-849, doi:10.1130/B35133.1.

LIANG, W., GARZANTI, E., ANDÒ, S., GENTILE, P., AND RESENTINI, A., 2019, Multimineral fingerprinting of Transhimalayan and Himalayan sources to Indus-derived Thal Desert sand (central Pakistan): Minerals, v. 9 (8), 457, doi:10.3390/min9080457.

MALLIK, T.K., 1978, Mineralogy of deep-sea sands of the Indian Ocean: Marine Geology, v. 27, p. 161-176.

MELLUSO, L., SETHNA, S.F., D’ANTONIO, M., JAVERI, P., AND BENNIO, L., 2002, Geochemistry and petrogenesis of sodic and potassic mafic alkaline rocks in the Deccan Volcanic Province, Mumbai area (India): Mineralogy and Petrology, v. 74(2-4), p. 323-342.

MILLIKEN, K.L., AND MACK, L.E., 1990, Subsurface dissolution of heavy minerals, Frio Formation sandstones of the ancestral Rio Grande Province, South Texas: Sedimentary Geology, v. 68(3), p. 187-199.

MORTON, A.C., AND HALLSWORTH, C., 2007, Stability of detrital heavy minerals during burial diagenesis, *in* Mange, M.A., and Wright, D.T., eds., Heavy Minerals in Use: Amsterdam, Elsevier, Developments in Sedimentology Series 58, p.215-245.

MORTON, A.C., AND MCGILL, P., 2018, Correlation of hydrocarbon reservoir sandstones using heavy mineral provenance signatures: Examples from the North Sea and adjacent areas: Minerals, v. 8 (12), 564, doi:10.3390/min8120564.

MUNACK, H., KORUP, O., RESENTINI, A., LIMONTA, M., GARZANTI, E., BLÖTHE, J.H., SCHERLER, D., WITTMANN, H., AND KUBIK, P.W., 2014, Postglacial denudation of western Tibetan Plateau margin outpaced by long-term exhumation: Geological Society of America, Bulletin, v. 126, p. 1580-1594, doi:10.1130/B30979.1.

NAIR, N., AND PANDEY, D.K., 2018, Cenozoic sedimentation in the Mumbai Offshore Basin: Implications for tectonic evolution of the western continental margin of India: Journal of Asian Earth Sciences, v. 152, p. 132-144.

NAJMAN, Y., GARZANTI, E., PRINGLE, M., BICKLE, M., STIX, J., AND KHAN, I., 2003, Early-Middle Miocene paleodrainage and tectonics in the Pakistan Himalaya: Geological Society of America, Bulletin, v. 115, p. 1265–1277.

NAJMAN, Y., BICKLE, M., GARZANTI, E., PRINGLE, M., BARFOD, D., BROZOVICS, N., BURBANK, D., AND ANDÒ, S., 2009, Reconstructing the exhumation history of the Lesser Himalaya, NW India, from a multi-technique provenance study of the foreland basin Siwalik Formation: Tectonics, v. 28, TC5018, doi:10.1029/2009TC002506.

OHBA, T., AND NAKAGAWA, M., 2002, Minerals in volcanic ash 2: non-magmatic minerals: Global Environmental Research, v. 6(2), p. 53-60.

PANDEY, D.K., CLIFT, P.D., KULHANEK, D.K., AND THE EXPEDITION 355 SCIENTISTS, 2016a, Site U1456: Proceedings of the International Ocean Discovery Program 355, College Station (TX), doi.org/10.14379/iodp.proc.355.103.2016.

PANDEY, D.K., CLIFT, P.D., KULHANEK, D.K., AND THE EXPEDITION 355 SCIENTISTS, 2016b, Site U1457: Proceedings of the International Ocean Discovery Program 355, College Station (TX), doi.org/10.14379/iodp.proc.355.104.2016.

PANDEY, D.K., PANDEY, A., AND WHATTAM, S.A., 2019, Relict subduction initiation along a passive margin in the northwest Indian Ocean: Nature communications, 10:2248, doi.org/10.1038/s41467-019-10227-8.

PICKERING, K., CARTER, A., ANDÒ, S., GARZANTI, E., LIMONTA, M., VEZZOLI, G., AND MILLIKEN, K., 2020, Deciphering relationships between the Nicobar and Bengal Submarine Fans, Indian Ocean: Earth Planetary Science Letters, in Review.

REHMAN, S.S., SABIR, M.A., AND KHAN, J., 1997. Discharge characteristics and suspended load from rivers of Northern Indus Basin, Pakistan: Geological Bulletin University of Peshawar, v. 30, p. 325– 336.

ROUSE, H., 1937, Modern conceptions of the mechanics of fluid turbulence. Transactions of the American Society of Civil Engineers, v. 102, p. 463–543.

SUCZEK, C.A., AND INGERSOLL, R.V., 1985, Petrology and provenance of Cenozoic sand from the Indus cone and the Arabian Basin, DSDP Sites 221, 222, and 224: Journal of Sedimentary Petrology, v. 55, p. 340- 346.

SZULC, A.G., NAJMAN, Y., SINCLAIR, H. D., PRINGLE, M., BICKLE, M., CHAPMAN, H., GARZANTI, E., ANDÒ, S., HUYGHE, P., MUGNIER, J.L., OJHA, T., AND DECELLES, P., 2006, Tectonic evolution of the Himalaya constrained by detrital ^{40}Ar–^{39}Ar, Sm–Nd and petrographic data from the Siwalik foreland basin succession, SW Nepal: Basin Research, v. 18, p. 375-391.

TODAL, A., AND EDHOLM, O., 1998, Continental margin off western India and Deccan large igneous province: Marine Geophysical Researches, v. 20(4), p. 273-291.

WANG, J., HU, X., JANSA, L., AND HUANG, Z., 2011, Provenance of the Upper Cretaceous–Eocene deep-water sandstones in Sangdanlin, southern Tibet: Constraints on the timing of initial India-Asia collision: Journal of Geology, v. 119, p. 293–309.

WEEDON, G. P., AND McCAVE, I. N., 1991, Mud turbidites from the Oligocene and Miocene Indus Fan at Sites 722 and 731 on the Owen Ridge, *in* Prell, W. L., Niitsuma, N., et al., Proceedings of the Ocean Drilling Program, Scientific Results: College Station, Texas, Ocean Drilling Program, v. 117, p. 215–229.

WHITE, N., PRINGLE, M., GARZANTI, E., BICKLE, M., NAJMAN, Y., CHAPMAN, H., AND FRIEND, P., 2002, Constraints on the exhumation and erosion of the High Himalayan slab, NW India, from foreland basin deposits: Earth Planetary Science Letters, v. 195, p. 29-44.

Figure 4

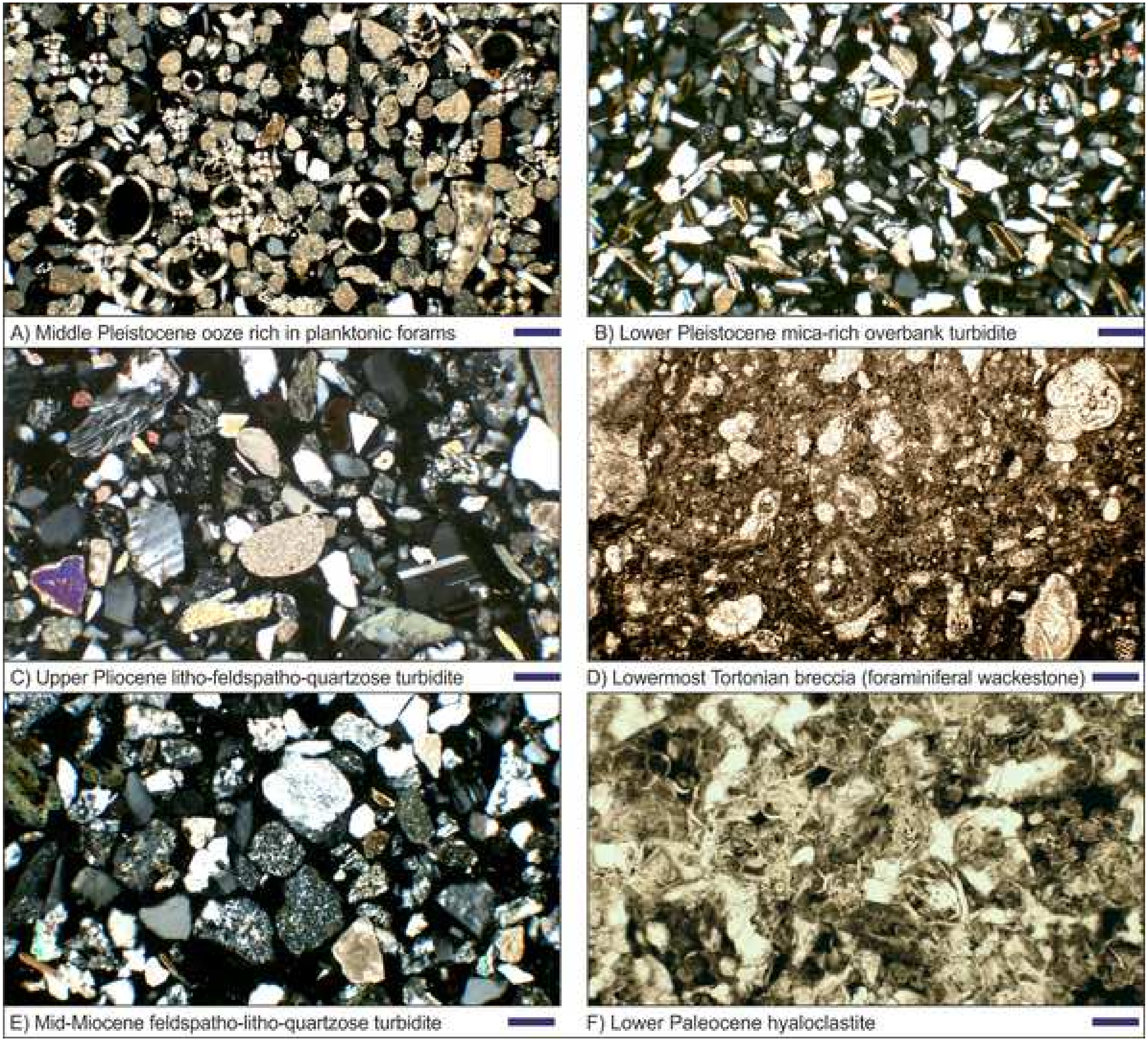

A) Middle Pleistocene ooze rich in planktonic forams

B) Lower Pleistocene mica-rich overbank turbidite

C) Upper Pliocene litho-feldspatho-quartzose turbidite

D) Lowermost Tortonian breccia (foraminiferal wackestone)

E) Mid-Miocene feldspatho-litho-quartzose turbidite

F) Lower Paleocene hyaloclastite

Figure 5

A: INDUS FAN TOP
brown augite
green augite
hypersthene
glaucophane
forams with pyrite
phosphate grains
B: INDUS FAN MAIN TURBIDITE BODY
hornblende
kyanite
clinopyroxenes
epidote
garnet
0 µm 100
hypersthene
staurolite
titanite
C: NATARAJA SLIDE
apatite
fish tooth
garnet
brown augite
glaucony
D: BASAL TURBIDITE
hornblende
epidote
Cr-spinels
titanite
E: LOWER PALEOCENE MUDROCKS
apatite needle
Cr-rich & pyrope garnets
barite
fish tooth
volcanic glass
aegirine
sphalerite

Figure 6

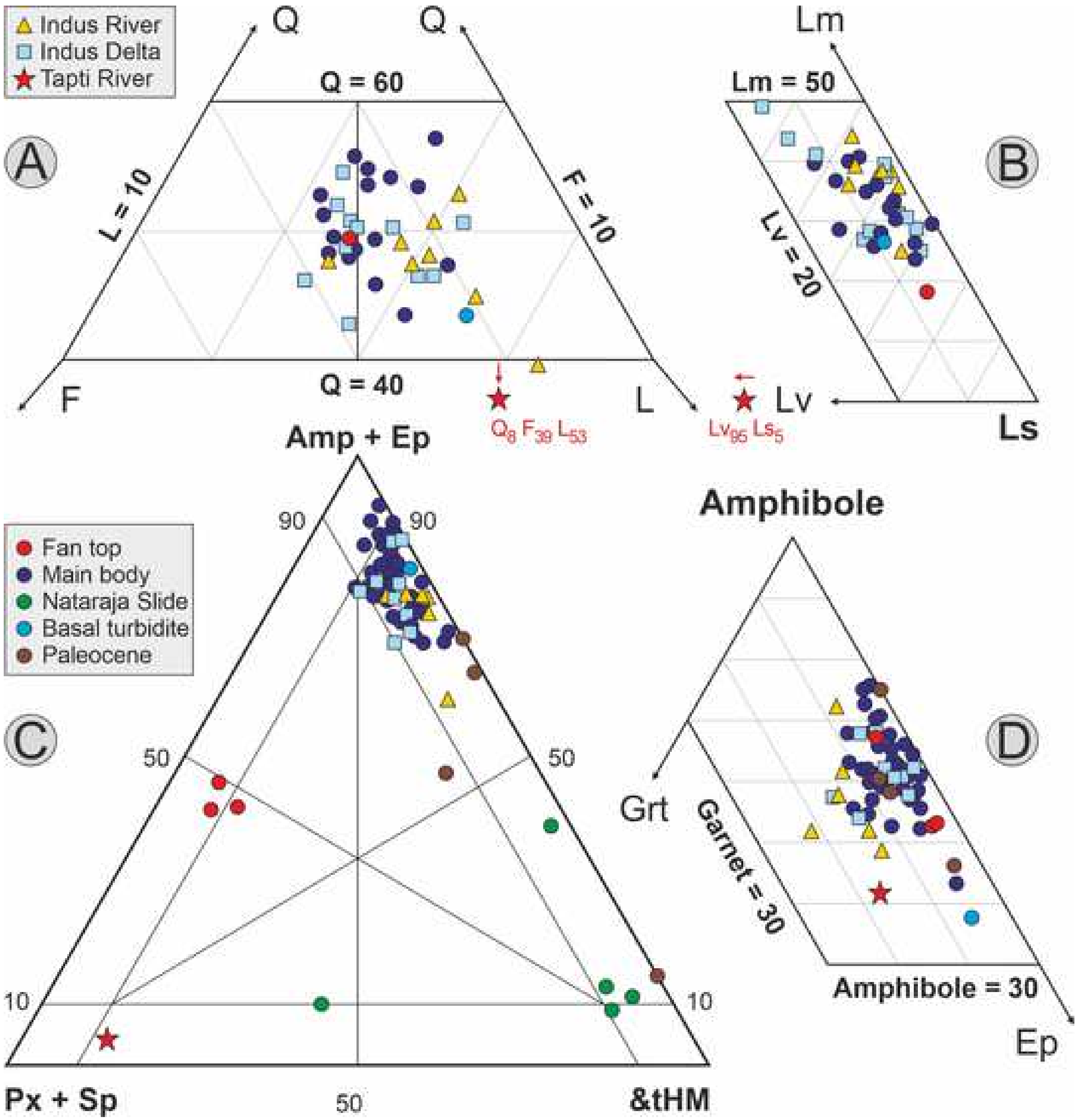

Indus River
Indus Delta
Tapti River
A
Q
Q
Q = 60
L = 10
F = 10
Q = 40
F
L
Q8 F39 L53
B
Lm
Lm = 50
Lv = 20
Lv
Ls
Lv95 Ls5
Amp + Ep
C
Fan top
Main body
Nataraja Slide
Basal turbidite
Paleocene
90
90
50
50
10
10
Px + Sp
50
&tHM
Amphibole
D
Grt
Garnet = 30
Amphibole = 30
Ep

Figure 1

Click here to access/download;Figure;Figure 1 IndusFan Sites.jpg

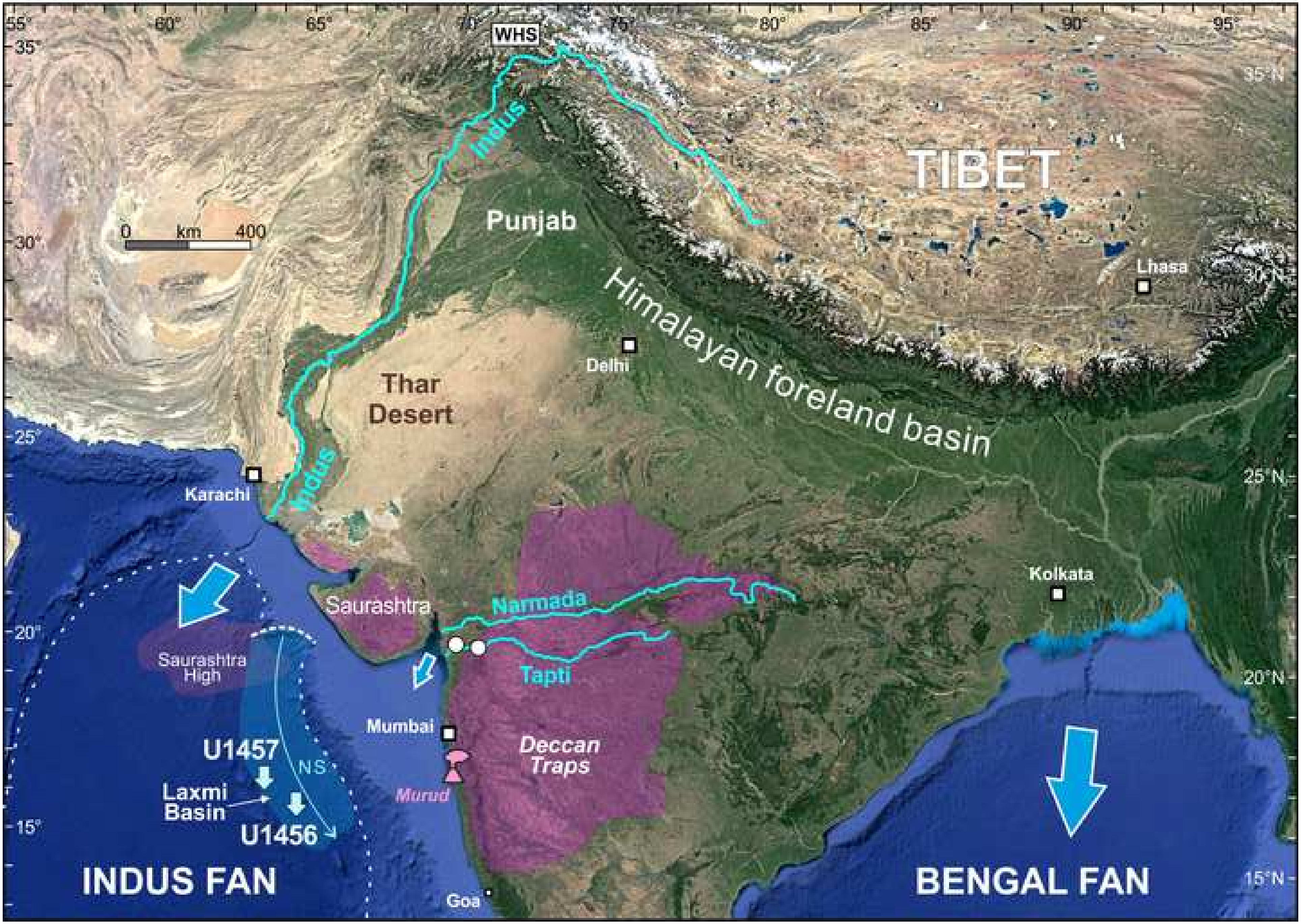

Figure 2

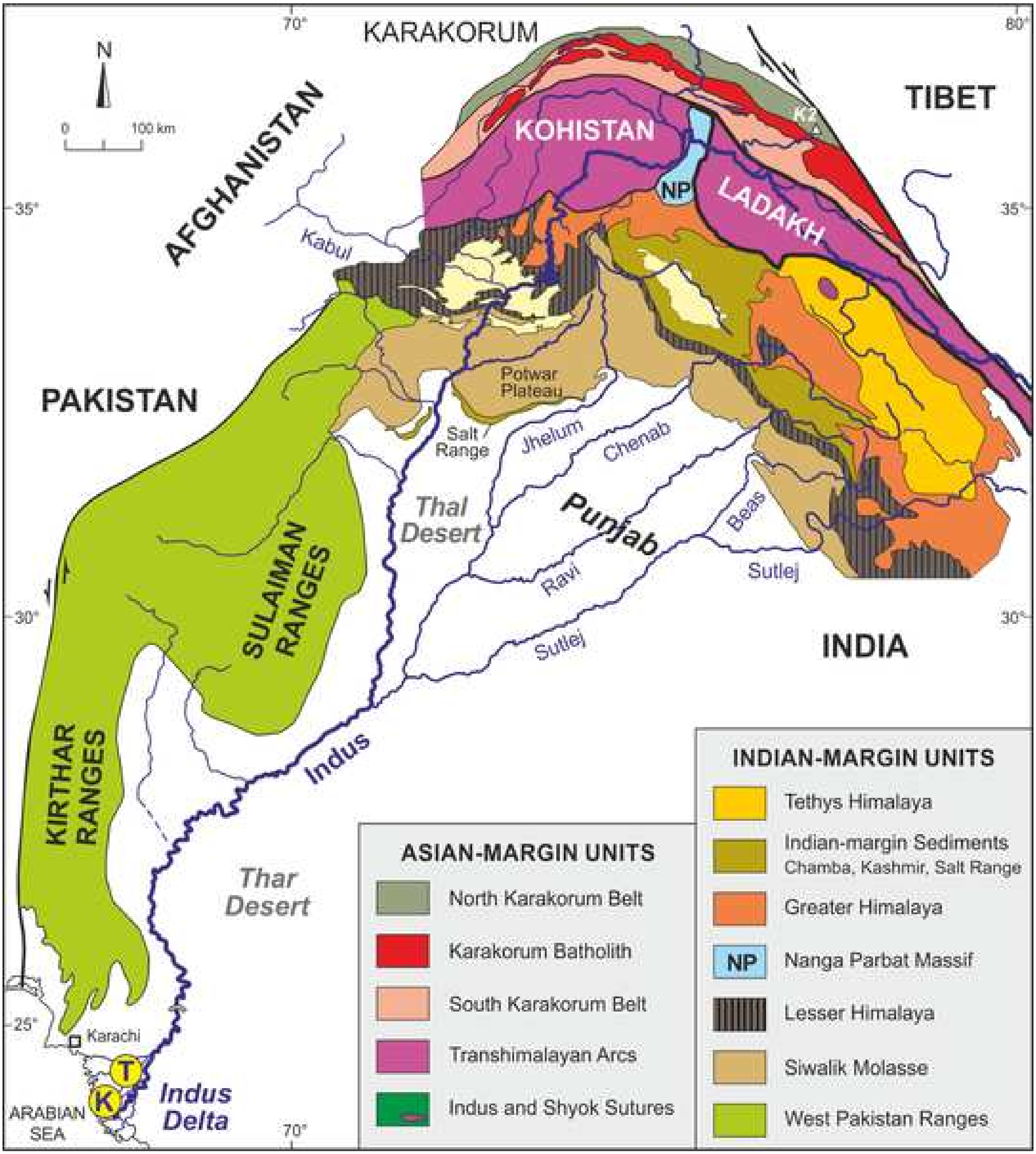

70°
80°
35°
30°
25°
N
0
100 km
KARAKORUM
TIBET
AFGHANISTAN
KOHISTAN
K2
NP
LADAKH
Kabul
PAKISTAN
Potwar Plateau
Salt Range
Jhelum
Chenab
Thal Desert
Punjab
Beas
Ravi
Sutlej
SULAIMAN RANGES
INDIA
KIRTHAR RANGES
Indus
Thar Desert
Karachi
T
K
ARABIAN SEA
Indus Delta
ASIAN-MARGIN UNITS
North Karakorum Belt
Karakorum Batholith
South Karakorum Belt
Transhimalayan Arcs
Indus and Shyok Sutures
INDIAN-MARGIN UNITS
Tethys Himalaya
Indian-margin Sediments
Chamba, Kashmir, Salt Range
Greater Himalaya
Nanga Parbat Massif
Lesser Himalaya
Siwalik Molasse
West Pakistan Ranges

Figure 3

Click here to access/download;Figure;Figure 3 IndusFan Pies.jpg

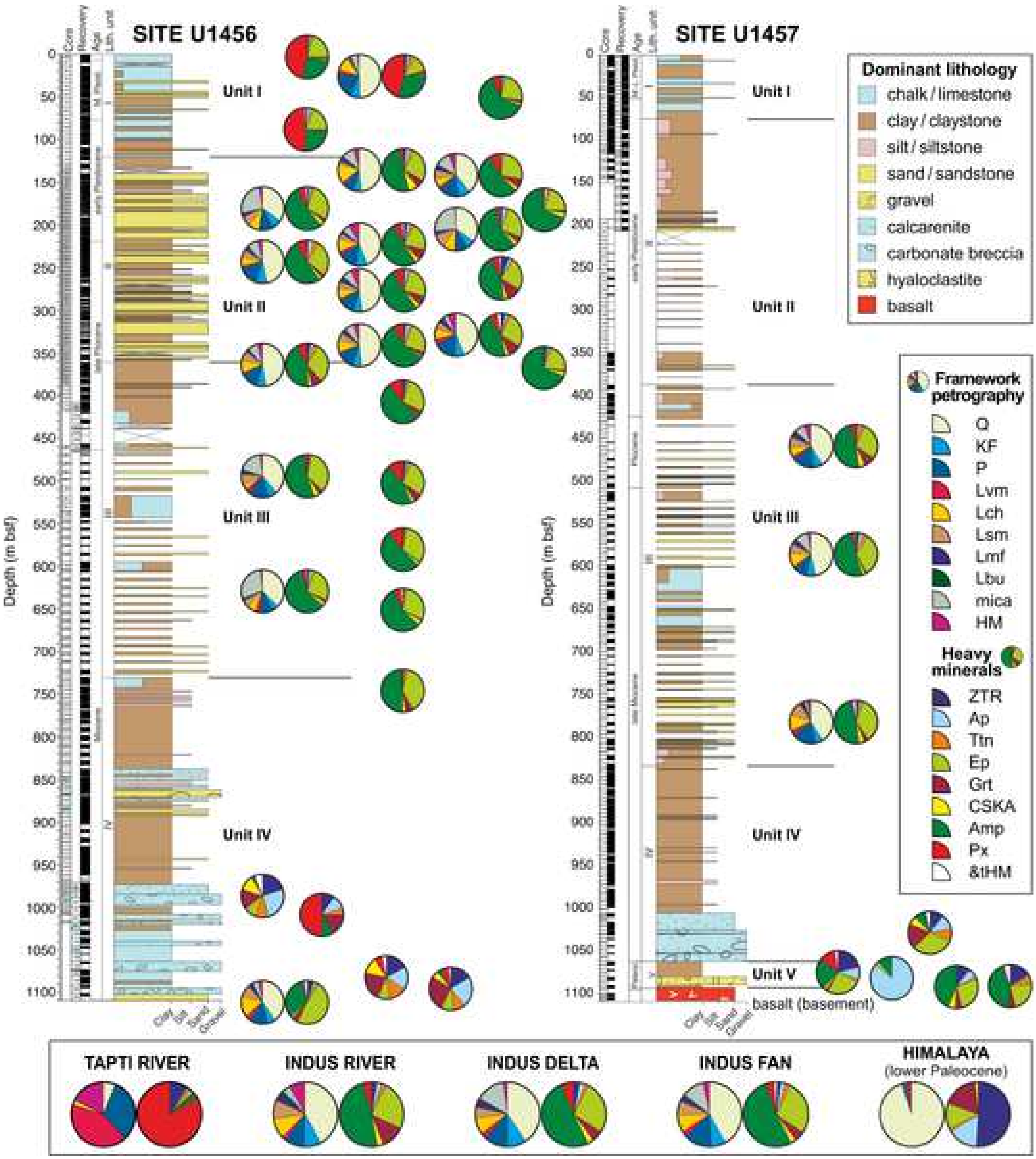

Table 1

Unit	Source	N°	Q	KF	P	Lv	Lc	&Lsm	Lmf	Lbu	mica	HM	
RECENT SANDS													
Modern Tapti River	*1*	1	7	0	32	41	2	0	0	0	0	17	100.0
Modern Indus River	*2*	10	42	9	10	2	10	9	4	2	3	9	100.0
Holocene Indus Delta	*3*	9	40	9	12	3	9	5	4	0	16	2	100.0
LAXMI BASIN													
Fan top	*1*	1	49	7	20	3	10	1	2	0	6	1	100.0
Main body	*1*	15	42	7	13	2	8	7	3	0	12	4	100.0
Main body	*5*	1	49	5	9	2	14	2	3	1	10	4	100.0
Base of slide	*1*	1	40	6	13	4	16	9	3	1	4	3	100.0
TETHYS HIMALAYA	*6*	13	94	1	1	2	0	1	1	0	0	0	100.0

Unit	Source	N°	tHMC	ZTR	Ap	Ttn	Ep	Grt	CSKA	Amp	Px	&tHM	
RECENT SANDS													
Modern Tapti River	*1*	1	18	9	0	1	2	1	1	2	84	0	100.0
Modern Indus River	*2*	6	8	3	2	2	25	12	3	49	4	0.2	100.0
Holocene Indus Delta	*3*	10	3	3	2	2	27	6	3	51	6	0.1	100.0
LAXMI BASIN													
Fan top	*1*	3	2	2	2	3	18	2	1	26	47	0.4	100.0
Main body	*1*	16	6	2	2	2	27	6	3	51	6	1	100.0
Main body	*4*	13	4	3	3	4	28	4	2	51	4	0.2	100.0
Main body	*5*	9	2	1	1	2	27	3	3	57	4	0.5	100.0
Nataraja slide	*1*	5	0.03	15	17	9	12	19	7	5	13	3	100.0
Base of slide	*1*	1	3	5	2	2	49	5	1	33	1	2	100.0
Paleocene mudrocks	*1*	4	0.04	12	25	3	19	3	2	30	4	2	100.0
TETHYS HIMALAYA	*6*	10	0.1	51	15	2	13	17	0	0	0	1	100.0

Appendix Tables Captions

Appendix Table A1

Appendix Table A2

Appendix Table A3

Click here to access/download
Supplemental Material
Appendix Table A3 Indus Fan Heavy Minerals.pdf

Sample Location